Article

Journal of Nanoscience and Nanotechnology
Vol. 15, 8749–8755, 2015
www.aspbs.com/jnn

Silicon Surface Modification Using $C_4F_8 + O_2$ Plasma for Nano-Imprint Lithography

Junmyung Lee[1], Alexander Efremov[2], Jaemin Lee[1], Geun Young Yeom[3], and Kwang-Ho Kwon[1,*]

[1] *Department of Control and Instrumentation Engineering, Korea University, Sejong 339-700, South Korea*
[2] *Department of Electronic Devices and Materials Technology, State University of Chemistry and Technology, 7 Sheremetevsky Prosp., 153000 Ivanovo, Russia*
[3] *Department of Advanced Materials Science and Engineering, Sungkyunkwan University, Suwon 440-746, South Korea*

The investigation of $C_4F_8+O_2$ feed gas composition on both plasma parameters and plasma treated silicon surface characteristics was carried out. The combination of plasma diagnostics by Langmuir probes and plasma modeling indicated that an increase in O_2 mixing ratio results in monotonically decreasing densities of CF_x ($x = 1$–3) radicals as well as in non-monotonic behavior of F atom density. The surface characterization by X-ray photoelectron spectroscopy and contact angle measurements showed that the $C_4F_8+O_2$ mixtures with less than 60% O_2 result in modification of Si surfaces due to the deposition of the FC polymer films while the change of O_2 mixing ratio in the range of 30%–60% provides an effective adjustment of the surface characteristics such as surface energy, contact angle, etc.

Keywords: C_4F_8 Plasma, Treatment, Fluorocarbon Polymer, Surface Modification.

1. INTRODUCTION

Nano-imprint lithography (NIL) is one of the promising technologies for fast reproducing nano-scale patterns on the large-area wafers.[1,2] In this technology, the mold made from silicon, silicon dioxide or quartz is simply pressed into a resist and then, is released back leaving the required pattern in the mask. Since the resist often adheres to the mold, the NIL process suffers from several critical problems such as pattern deformation, non-uniform printing and production of residual layers.[3] In fact, all these problems are connected with the mold quality. That is why, the optimization of the mold properties is very important for improving the overall NIL technology.

Generally, in order to minimize the adhesion of resist to the mold surface, the mold needs to have low surface energy. Several researches have studied the modification of the mold surfaces by the polymer-forming fluorocarbon plasmas.[4,5] Particularly, it was found that, after the plasma treatment, the mold surface characteristics are strongly determined by the thickness and chemical composition of the deposited fluorocarbon (FC) polymer film. It is obvious that the properties of the FC polymer film (and thus, the properties of the mold itself), may be adjusted by plasma parameters, type and composition of a feed gas. Unfortunately, in published works, the relationship between the plasma parameters and the polymer characteristics were not investigated in detail. Such situation retards the development of NIL technology.

In this work, we attempted both experimental and model-based study of the relationships between the initial composition of $C_4F_8 + O_2$ gas mixture, densities of plasma active species and properties of Si surfaces treated with different C_4F_8/O_2 mixing ratios. The choice of C_4F_8 was because it is known as a strongly polymerizing gas under the plasma conditions.[6–8] At the same time, the O_2 is frequently used as the additive gas in fluorocarbon-based plasmas for suppressing the polymerization.[6–8] Therefore, it can be expected that the variation in C_4F_8/O_2 mixing ratio at constant total gas pressure and input power may be an effective tool for adjusting the properties of the deposited FC polymer films.

*Author to whom correspondence should be addressed.

1533-4880/2015/15/8749/007
doi:10.1166/jnn.2015.11511

2. EXPERIMENTAL DETAILS AND MODELING

2.1. Experimental Setup and Procedures

The experiments were performed in a planar inductively coupled plasma (ICP) reactor with a cylindrical chamber ($r = 15$ cm), made from anodized aluminum. A 5-turn-copper coil was located on the top of the chamber, above the 10-mm-thick horizontal quartz window. The coil was connected to a 13.56 MHz power supply in order to sustain the plasma. The distance between the window and the bottom electrode, which was used as a substrate holder, was $l = 12.8$ cm. Since the bottom electrode was not biased, it appeared under the floating potential. During the experiments, we used a fixed total gas flow rate ($q = 30$ sccm), gas pressure ($p = 10$ mTorr), and input power ($W_{\text{inp}} = 600$ W). The input power density $W' = W_{\text{inp}}/\pi r^2 l$ then became 0.6 W/cm^3. The $C_4F_8+O_2$ gas compositions were set by adjusting the partial flow rates.

The Si(100) samples with the size of about 2×2 cm^2 were placed in the center of the bottom electrode. The temperature of the bottom electrode was stabilized at 17 °C using a water-flow cooling system. The processing time τ was 30 s. Both treated and reference (non-treated) silicon surfaces were examined using the X-ray photoelectron spectroscopy (XPS) and contact angle measurements. The XPS was provided by VG Scientific ESCALAB 200R with Mg K_α 1253.6 eV radiation operating at 260 W. The binding energies were calibrated using C(1s) peak at 284.5 eV. The contact angles were measured at room temperature using the drop shape analysis system (DSA-100, KRUSS) with polar (de-ionized water) and non-polar (CH_2I_2) liquids. Then, the free surface energy was calculated through the Owens-Wendt equation.[9]

The plasma parameters were determined by a double Langmuir probe (LP), (DLP2000, Plasmart Inc.). The probe tip was installed through a hole in the sidewall of the chamber, 5.7 cm above the bottom electrode and centered in a radial direction. In order to ensure that the LP results were not affected by the formation of the FC polymer film on the tip surface, the probe tip was cleaned in 50% Ar+ 50% O_2 plasma before and after each measurement. The preliminary experiments showed that, even for pure C_4F_8 plasma, the differences between the continuously recorded current–voltage (I–V) curves did not exceed the standard experimental error for a period of at least 2 min after the plasma was turned on. Since this time was more than τ, the measured LP data were adequate to the treatment conditions. The raw I–V curves were treated using the Johnson & Malter's double probe theory[10] and the Allen-Boyd-Reynolds (ABR) approximation for the ion saturation current density.[11] These assume $J_+ \approx 0.61 e n_+ \upsilon$, where υ is the ion Bohm velocity. The effective ion mass needed to determine υ was evaluated simply through the mole fractions of the corresponding neutral species. The output LP data were the electron temperature (T_e), ion current density (J_+), floating potential (U_f), and total positive ion density (n_+).

2.2. Plasma Modeling

To obtain the densities and fluxes of the active species, we developed a simplified zero-dimensional model operating with the volume-averaged plasma parameters. Similar to our papers,[12,13] the model was based on the Maxwellian electron energy distribution function (EEDF), and used the experimental results of T_e and n_+ directly as input parameters. Earlier, it was found that, for the given range of process conditions, the electronegativity of both C_4F_8 and O_2 plasmas is low enough to assume $n_- \ll n_e \approx n_+$. Particularly, Vasenkov et al.[14] reported about $n_e \approx n_{CF_2^+} + n_{CF_3^+}$ in pure C_4F_8 and $n_e \approx n_{O_2^+}$ in pure O_2 at $p = 20$ mTorr and $W' = 0.5$ W/cm^3. Also, Rauf and Ventzek[15] measured $n_-/n_e \sim 0.06$ for 98% C_4F_8 + 2% Ar and $n_-/n_e \sim 0.03$ for 50% C_4F_8 + 50% Ar ICP at $p = 10$ mTorr and $W' = 0.6$ W/cm^3. And finally, Efremov et al.[16] noted $n_-/n_e \sim 0.2$ for pure O_2 ICP at $p = 10$ mTorr and $W' = 0.1$ W/cm^3. Since the last W' is much less than that in current study, we can assume $n_-/n_e < 0.1$ with confidence. That is why, our model accounted only for the chemistry of neutral species (Table I).[17–19]

The steady-state ($dn/dt = 0$) densities of neutral species were obtained from the system of chemical kinetics equations in the general form of $R_F - R_D = (k_s + 1/\tau_R)n$, where R_F and R_D are the volume-averaged formation and decay rates in bulk plasma for a given type of species, n is their density, k_S is the first-order heterogeneous decay rate coefficient, and $\tau_R = \pi r^2 l p/q$ is the residence time. The rate coefficients for electron impact reactions (R1–R23), were calculated as functions of T_e using fitting expressions in the form of $k = AT_e^B \exp(-C/T_e)$.[17–19] The rate coefficients for R24–R63 were taken from the NIST chemical kinetics database.[20] The rate coefficients for the heterogeneous loss of atoms and radicals R64–R70 were calculated as $k_S = [(\Lambda^2/D) + (2r/\gamma\upsilon_T)]^{-1}$, where D is the effective diffusion coefficient,[30] $\Lambda^{-2} = (2.405/r)^2 + (\pi/l)^2$ is the diffusion length,[21] and $\upsilon_T = (8k_B T/\pi m)^{1/2}$. The sticking probabilities γ were obtained from Refs. [16, 17]. The temperature of the neutral ground-state species T was assumed to be independent of the feed gas composition.[16–18] Since experimental data on T were not extracted during this study, we took $T = 700$ K as the typical value for close ranges of p and W' in ICP etching reactors with similar geometry.[16,17] All reaction pathways between the adsorbed (marked by the "s" index) and gaseous species inside R64–R69 were assumed to have equal probabilities of occurrence. The rate coefficients for the heterogeneous loss of ions R71–R73 were calculated as $k_S = \upsilon/d_c$, where $d_c = 0.5rl/(rh_l + lh_r)$. The correction factors for axial (h_l) and radial (h_r) sheath sizes are given by the low pressure diffusion theory.[21]

Table I. Reduced reaction set for the modeling of neutral species chemistry in $C_4F_8 + O_2$ plasmas.

Process		Rate coefficient [cm^3/s]			
		ε_{th} [eV]	A	B	C
Electron-impact reactions					
R1	$C_4F_8 + e = 2C_2F_4 + e$	2.16	8.71×10^{-8}	0.042	8.572
R2	$C_4F_8 + e = C_3F_6 + CF_2 + e$	3.25	8.71×10^{-8}	0.042	8.572
R3	$C_3F_6 + e = C_2F_4 + CF_2 + e$	4.53	1.07×10^{-8}	0.23	7.451
R4	$C_2F_4 + e = 2CF_2 + e$	3.06	1.32×10^{-8}	0.412	6.329
R5	$C_2F_4 + e = C_2F_3^+ + F + 2e$	15.57	3.03×10^{-9}	0.874	16.41
R6	$C_2F_3 + e = CF_2 + CF + e$	3.06	3.30×10^{-8}	0.412	6.329
R7	$CF_4 + e = CF_3 + F + e$	5.60	1.38×10^{-8}	0	16
R8	$CF_4 + e = CF_2 + 2F + e$	9.50	2.22×10^{-10}	0.99	14.77
R9	$CF_4 + e = CF_3^+ + F + 2e$	15.9	9.36×10^{-8}	0	20.4
R10	$CF_4 + e = CF_3 + F^+ + 2e$	23.10	9.79×10^{-10}	0.94	34.67
R11	$CF_3 + e = CF_2 + F + e$	3.80	6.48×10^{-8}	−0.959	11.25
R12	$CF_2 + e = CF + F + e$	5.40	8.11×10^{-9}	0.386	8.739
R13	$CF_2 + e = C + 2F + e$	11.00	1.39×10^{-8}	−1.164	49.87
R14	$CF + e = C + F + e$	5.60	1.63×10^{-8}	−0.002	13.05
R15	$F_2 + e = 2F + e$	4.34	1.08×10^{-8}	−0.296	4.464
R16	$O_2 + e = 2O + e$	6.40	1.52×10^{-9}	0	4.15
R17	$O_2 + e = O + O(1d) + e$	8.57	2.04×10^{-8}	0	8.18
R18	$CO_2 + e = CO + O + e$	13.50	1.87×10^{-8}	0	13.89
R19	$CO + e = C + O + e$	13.50	1.87×10^{-8}	0	13.89
R20	$O + e = O(1d) + e$	1.97	4.47×10^{-9}	0	2.29
R21	$FO + e = F + O + e$	4.30	6.16×10^{-9}	0	4.30
R22	$CFO + e = CO + F + e$	5.40	8.11×10^{-9}	0.386	8.739
R23	$CF_2O + e = CFO + F + e$	3.80	6.48×10^{-8}	−0.959	11.25
Bulk atom–molecular, radical–molecular and radical–radical reactions					
R24	$C_2F_3 + F = C_2F_4$	1.00×10^{-12}			
R25	$C_2F_4 + O = CF_2O + CF_2$	2.51×10^{-12}			
R26	$C_2F_4 + O(1d) = CF_2O + CF_2$	2.51×10^{-11}			
R27	$C_2F_4 + F = CF_2 + CF_3$	3.98×10^{-11}			
R28	$C_2F_4 + C = C_2F_3 + CF$	1.00×10^{-10}			
R29	$F_2 + CF_3 = CF_4 + F$	6.31×10^{-14}			
R30	$F_2 + CF_2 = CF_3 + F$	7.94×10^{-14}			
R31	$F_2 + CF = CF_2 + F$	3.98×10^{-12}			
R32	$F_2 + O = FO + F$	1.00×10^{-16}			
R33	$F_2 + O(1d) = FO + F$	7.94×10^{-12}			
R34	$F_2 + CFO = CF_2O + F$	5.01×10^{-14}			
R35	$CF_3 + F = CF_4$	1.00×10^{-12}			
R36	$CF_3 + O = CF_2O + F$	3.16×10^{-11}			
R37	$CF_3 + O(1d) = CF_2O + F$	3.16×10^{-11}			
R38	$CF_2 + F = CF_3$	4.17×10^{-13}			
R39	$2CF_2 = C_2F_4$	5.01×10^{-14}			
R40	$CF_2 + CF = C_2F_3$	1.00×10^{-12}			
R41	$CF_2 + O = CFO + F$	3.16×10^{-11}			
R42	$CF_2 + O(1d) = CFO + F$	3.16×10^{-11}			
R43	$CF_2 + O = CO + 2F$	3.98×10^{-12}			
R44	$CF_2 + O(1d) = CO + 2F$	3.98×10^{-12}			
R45	$CF + F = CF_2$	5.01×10^{-15}			
R46	$CF + O = CO + F$	6.31×10^{-11}			
R47	$CF + O(1d) = CO + F$	2.00×10^{-11}			
R48	$CF + O_2 = CFO + O$	3.16×10^{-11}			
R49	$FO + O = F + O_2$	2.51×10^{-11}			
R50	$FO + O(1d) = F + O_2$	5.01×10^{-11}			
R51	$FO + FO = 2F + O_2$	2.51×10^{-12}			
R52	$2FO = F_2 + O_2$	2.51×10^{-16}			
R53	$CFO + CF_3 = CF_4 + CO$	1.00×10^{-11}			
R54	$CFO + CF_3 = CF_2O + CF_2$	1.00×10^{-11}			
R55	$CFO + CF_2 = CF_3 + CO$	3.16×10^{-13}			
R56	$CFO + CF_2 = CF_2O + CF$	3.16×10^{-13}			
R57	$CFO + O = CO_2 + F$	1.00×10^{-10}			
R58	$CFO + O(1d) = CO_2 + F$	1.00×10^{-10}			
R59	$2CFO = CF_2O + CO$	1.00×10^{-11}			

Table 1. Continued.

Process		Rate coefficient [cm^3/s]			
		ε_{th} [eV]	A	B	C
R60	$CFO + F = CF_2O$	7.94×10^{-11}			
R61	$CF_2O + O(1d) = F_2 + CO_2$	2.00×10^{-11}			
R62	$C + O_2 = CO + O$	1.58×10^{-11}			
R63	$CO + F = CFO$	1.29×10^{-11}			
Heterogeneous reactions					
R64	$F = F(s) + CF_3 = CF_4$	$f(\gamma)$, $\gamma = 0.05$			
	$+ CF_2 = CF_3$				
	$+ CF = CF_2$				
	$+ F = F_2$				
	$+ C = CF$				
	$+ C_2F_3 = C_2F_4$				
	$+ O = FO$				
R65	$CF_3 = CF_3(s) + F = CF_4$	$f(\gamma)$, $\gamma = 0.05$			
	$+ CF = C_2F_4$				
	$+ C = C_2F_3$				
R66	$CF_2 = CF_2(s) + F = CF_3$	$f(\gamma)$, $\gamma = 0.1$			
	$+ CF_2 = C_2F_4$				
	$+ CF = C_2F_3$				
	$+ O = CF_2O$				
R67	$CF = CF(s) + F = CF_2$	$f(\gamma)$, $\gamma = 0.1$			
	$+ CF_2 = C_2F_3$				
	$+ CF_3 = C_2F_4$				
	$+ O = CFO$				
R68	$C = C(s) + F = CF$	$f(\gamma)$, $\gamma = 1$			
	$+ CF_3 = C_2F_3$				
	$+ O = CO$				
R69	$O = O(s) + O = O_2$	$f(\gamma)$, $\gamma = 0.1$			
	$+ F = FO$				
	$+ C = CO$				
	$+ CF = CFO$				
	$+ CF_2 = CF_2O$				
R70	$O(1d) = O$	$f(\gamma)$, $\gamma = 1$			
R71	$CF_3^+ = CF_3$	υ/d_c, where $\upsilon \approx \sqrt{eT_e}/m_i$ $d_c = 0.5rl/(rh_l + lh_r)$			
R72	$F^+ = F$				
R73	$C_2F_3^+ = C_2F_3$				

The model quality was preliminarily tested using the experimental data on both CF_2 and CF radical densities in C_4F_8/Ar plasma from Ref. [15]. This work was selected because it also provides the measurements of T_e and n_e, which are required as input model parameters. As a result, the reasonable agreement between measured and model-predicted densities was obtained.

3. RESULTS AND DISCUSSION

3.1. Plasma Characterization

Figure 1 represents the results of plasma diagnostics using Langmuir probes. From Figure 2, it can be seen that an increase in O_2 fraction in a feed gas results in decreasing T_e in the ranges of 3.5–3.2 eV. The reason for this is an increase in the electron energy loss due to the low-threshold excitations (vibrational, electronic) for O_2 and other molecular species, which appear in a gas phase as products of plasma chemical reactions. The measured total density of positive ions (and thus, the electron density,

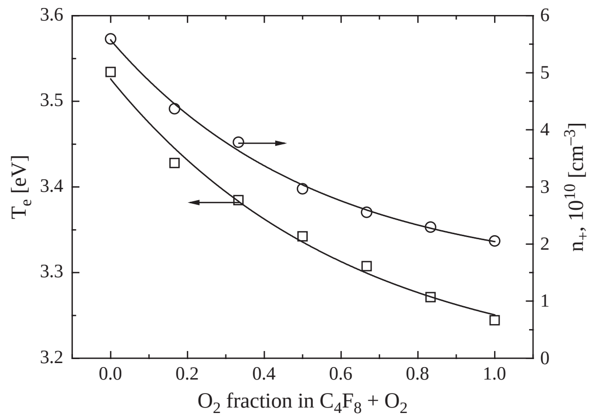

Figure 1. Measured electron temperature (T_e) and total positive ion density (n_+) as functions of O_2 fraction in $C_4F_8+O_2$ gas mixture. The remaining process conditions are $p = 10$ mTorr, $W_{inp} = 600$ W and $q = 30$ sccm.

since $n_+ \approx n_e$) also decreases toward O_2-rich plasmas ($n_+ = 5.6\times10^{10}$–2.1×10^{10} cm^{-3} for 0–100% O_2). In our opinion, such effects are caused by a combination of at least two phenomena. First, the decreasing T_e suppresses ionization through decreasing the ionization rate coefficients k_{iz} for all types of neutral species. The high sensitivity of k_{iz} to T_e is because $\varepsilon_{iz} \approx 12$–$15$ eV $> \langle\varepsilon\rangle$, where ε_{iz} is the threshold energy for ionization,[17,19] and $\langle\varepsilon\rangle = (3/2)T_e$ is the mean electron energy for Maxwellian EEDF. And secondly, the substitution of Ar for O_2 probably results in an increase in the densities of electronegative species, caused by both the O_2 itself and oxygen-containing reaction products. This accelerates the decay of the positive ions and electrons through ion–ion recombination and dissociative attachment, respectively. It is important to note also that the behaviors of both T_e and n_+ versus O_2 mixing ratio shown in Figure 1 are in good qualitative agreement with previously published data.[14,22]

Figure 2 illustrates the influence of O_2 content in the $C_4F_8+O_2$ gas mixture on the densities of neutral species. In pure C_4F_8 plasma, the dominant neutral species are C_2F_4, C_2F_3 and CF_x ($x = 1$–3) radicals. The high densities of C_2F_4, C_2F_3 and CF_2 are related with the direct formation of these species in R1–R6 with the participation of the original C_4F_8 molecules and their first-step dissociation products. The domination of CF_2 over other types of neutral species results from the significant contribution to their total formation rate from the sides of R27, R31, and R45. The high formation rate and density of CF_3 radicals is provided not only by the primary electron-impact reactions R7 and R10, but also by R27, R38, and R66 because of the high densities of C_2F_4 and CF_2, respectively. And finally, the density of CF radicals is lifted up due to their high formation rates in electron-impact reactions R6 and R12 with the participation of C_2F_3 and CF_2. The combination of high values of n_{CF_3}, n_{CF_2} and n_{CF} makes the C_4F_8 plasma a strongly polymerizing system. This fact has been repeatedly confirmed by experiment.[18,23,24] The addition of O_2 to C_4F_8 introduces additional dissociation mechanisms for C_2F_4 (R25, R26), CF_3 (R36, R37), CF_2 (R41–R44) and CF (R46–R48) increasing the total loss ràtes for these species compared with non-oxygenated plasmas. As a result, their densities (Fig. 2) and fluxes (Fig. 3) decrease faster that linearly (for example, by 8 times for CF_2 at 0–50% O_2) with increasing O_2 fraction in a feed gas. Simultaneously, since the reactions R36, R37, R41–R44 and R46–R48 follow the scheme of $CF_x + O \rightarrow CF_{x-1}O + F$, the addition of O_2 accelerated the formation of F atoms and results in

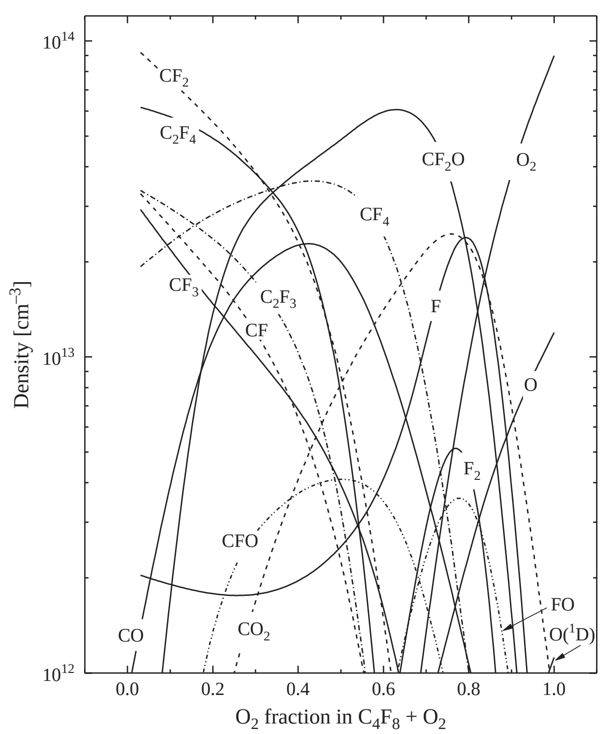

Figure 2. Model-predicted densities of neutral species as functions of O_2 fraction in $C_4F_8+O_2$ gas mixture. The process conditions correspond to Figure 1.

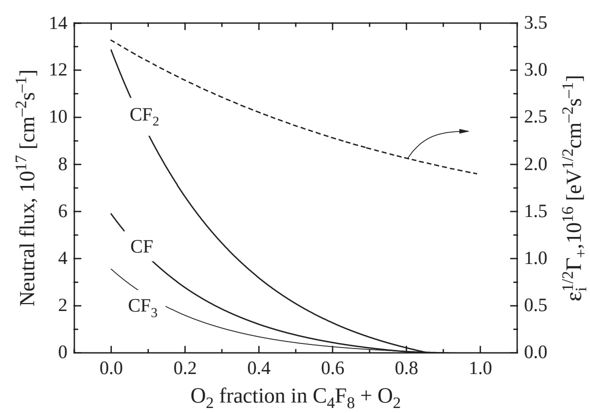

Figure 3. Model-predicted fluxes of polymer-forming species (CF_x radicals) and ion energy flux as functions of O_2 fraction in $C_4F_8+O_2$ gas mixture. The process conditions correspond to Figure 1.

the non-monotonic behavior of n_F. The ion energy flux characterized by the parameter $\sqrt{\varepsilon_i}\Gamma_+$,[12,25,26] where $\varepsilon_i \approx eU_f$—ion energy and $\Gamma_+ \approx J_+/e$—ion flux, also decreases toward O_2-rich plasmas. In our case, the low energy ions ($\varepsilon_i = 23$–19 eV for 0–100% O_2) cannot provide the sputtering of both FC film or Si surfaces. However, these can "open" the C–F bonds in the previously adsorbed fluorocarbon species ($\varepsilon_{C\text{–}F} = 552$ kJ/mol or 5.8 eV[27]) and thus, can increase the polymerization probability. Therefore, an increase in O_2 mixing ratio in the $C_4F_8 + O_2$ gas mixture definitely suppresses the deposition of the FC polymer film and shifts the general heterogeneous reaction pathway from polymerization to etching.

It is worth mentioning that the behaviors of the CF, CF_2, and CF_2O species shown in Figure 2 are in good agreement with the measured values reported by Li et al.[28] Also, the model-predicted fluxes of CF_x radicals from Figure 3 shows the same behavior with the FC film deposition rate[28] while the non-monotonic F atom flux corresponds to the non-monotonic Si etching rate.[28] All these allow us to conclude that our model provides an adequate description of the main kinetic effects determining the composition of $C_4F_8 + O_2$ plasma.

3.2. Surface Characterization

Figure 4 shows the C(1s) XPS narrow scan spectra for Si surfaces treated with different gas mixing ratios. It can be seen that the surface treated in 100% of C_4F_8 plasma shows the group of peaks in the range of 285–295 eV which belong to various fluorocarbon species. The presence of C–CF_x bonds at 287.0 eV directly points out on the polymer-like structure of the deposited film. An increase in O_2 fraction in a feed gas results in decreasing intensities for all fluorocarbon peaks while after 50% O_2 the C–C peak at 284.5 eV appear in the spectra. Since this peak was also detected on the reference (non-treated) surface as well as did not disappear (in fact, keep the same intensity) after the treatment in pure O_2 plasma, the observed carbon seems to be chemically bonded with Si atoms. This allows one to assume that, for the given treatment time, the $C_4F_8 + O_2$ mixtures with less than 50% O_2 provide the formation of the continuous FC polymer film on the Si surface.

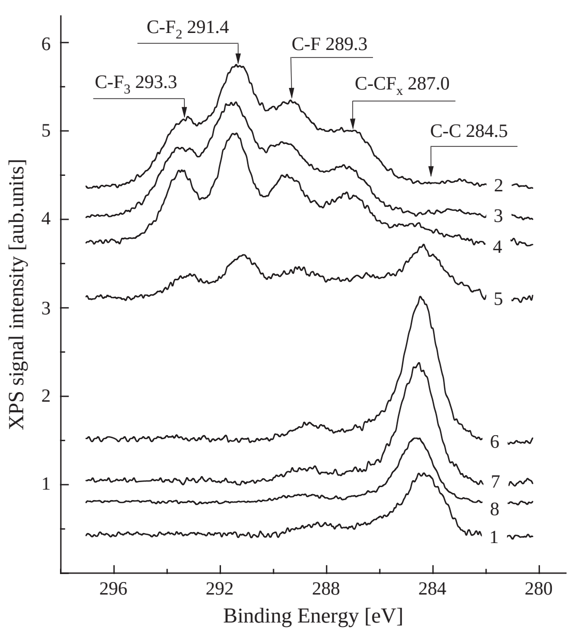

Figure 4. Measured C(1s) XPS narrow scan spectra for Si surfaces treated with different gas mixing ratios: 1-Reference (non-treated) sample, 2-100% C_4F_8, 3-83% $C_4F_8 + 17\%$ O_2, 4-67% $C_4F_8 + 33\%$ O_2, 5-50% $C_4F_8 + 50\%$ O_2, 6-33% $C_4F_8 + 67\%$ O_2, 7-17% $C_4F_8 + 83\%$ O_2, 8-100% O_2. The process conditions correspond to Figure 1.

Figure 5 illustrates the overall chemical states for Si surfaces calculated under an assumption that intensity of the XPS peak is proportional to the content of corresponding element. For this purpose, the C(1s), F(1s), O(1s) and Si(2p) peaks were used. It can be seen that the amount of C(1s) decreases monotonically toward O_2-rich plasmas that corresponds to the transition from C–F bonds in the FC polymer film to C–C bonds in the original surface. The fraction of F(1s) does not reflect the non-monotonic behavior of F atom density, but shows a good correlations with the total CF_x flux from Figure 3 as well as with the change of C(1s). The amount of bonded oxygen is one and the same for both reference (non-treated) samples and the samples treated in 100% O_2 plasma. Also, since the fraction of O(1s) decreases monotonically toward C_4F_8-rich plasmas following the behavior of Si(2p), one can conclude that the observed oxygen is not incorporated in the polymer film structure and belongs to the native silicon oxide. The disappearance of both O(1s) and Si(2p) peaks after the treatments with more than 70% C_4F_8 gas mixtures can be attributed to the formation of thick continuous FC polymer film. All these allow one to assume that the variations in O_2 content in a feed gas do not change the

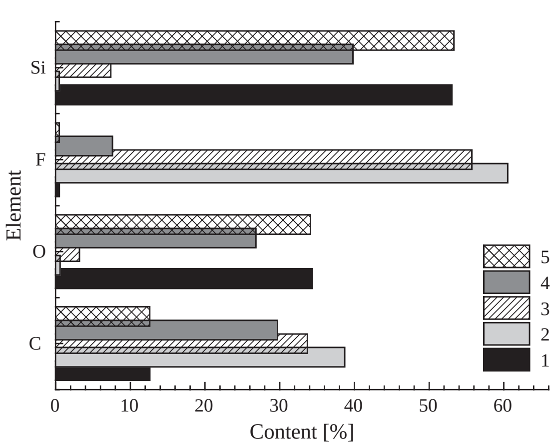

Figure 5. Chemical compositions for Si surfaces treated with different gas mixing ratios: 1-Reference (non-treated) sample, 2-100% C_4F_8, 3-67% $C_4F_8 + 33\%$ O_2, 4-33% $C_4F_8 + 67\%$ O_2, 5-100% O_2. The process conditions correspond to Figure 1.

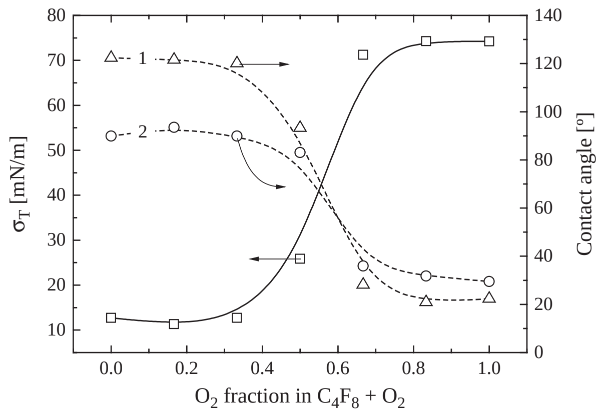

Figure 6. Measured contact angles (1-de-ionized water, 2-diiodomethane) and calculated free surface energy as functions of O_2 fraction in $C_4F_8 + O_2$ gas mixture. The process conditions correspond to Figure 1.

chemical structure of the FC polymer film, but influence the film thickness only.

From Refs. [9, 29], it is known that many surface characteristics (chemical activity, wettability, adhesion ability) are closely linked with the free surface energy σ_T. Speaking simply, the higher σ_T values correspond to "active" surface while the lower σ_T allows one to speak about an "inert" surface. From Figure 6, it can be seen that the transition from pure C_4F_8 to pure O_2 feed gas results in increasing σ_T in the range of 12.7–74.2 mN/m. This indicates that the plasma treated surface changes from the hydrophobic state to the hydrophilic one and/or becomes to be more adhesive for photoresists. The constancy of σ_T for less than 30% O_2 gas mixtures may be attributed to the formation of thick continuous FC polymer film with constant chemical composition. A rapid growth in σ_T for 30–60% O_2 is probably due to the transition to the non-continuous (island-like) film structure where an effective island size decreases with increasing O_2 fraction in a feed gas. Also, the same result may be obtained for thin continuous films if the film properties are affected by the substrate. And finally, the constancy of σ_T for more than 60% O_2 gas mixtures in our opinion corresponds to original Si surface with a negligible coverage by the FC polymer. Therefore, the $C_4F_8 + O_2$ mixtures with less than 60% O_2 result in modification of Si surfaces due to the deposition of the FC polymer films while the change of O_2 mixing ratio in the range of 30–60% provides an effective adjustment of the surface characteristics.

4. CONCLUSIONS

In this work, we carried out the Si surface modification by inductively coupled plasma C_4F_8/O_2 plasma treatment for the demolding process in nano-imprint lithography. We also investigated the influence of O_2 fraction in $C_4F_8 + O_2$ feed gas on both plasma parameters and plasma treated silicon surface characteristics. From plasma diagnostics by Langmuir probes and plasma modeling, it was found that the transition from C_4F_8-rich to O_2-rich plasmas results in monotonically decreasing densities and fluxes of polymer-forming species (CF_x radicals), but in non-monotonic behavior of F atom density. The XPS analysis showed that:
(1) the $C_4F_8 + O_2$ mixtures with less than 60% O_2 result in deposition of the FC polymer films; and
(2) the variations in O_2 mixing ratio influence the film thickness only. The measurements of free surface energy allow one to conclude that the change of O_2 mixing ratio in the range of 30–60% provides an effective adjustment of the surface characteristics. For less than 30% O_2 as well as for more than 60% O_2 the plasma treated surfaces keep the constant properties corresponding to thick continuous FC film (low σ_T) or original surface (high σ_T), respectively.

Acknowledgment: This study was supported by the Industrial Strategic Technology Development program (10041681, Development of fundamental technology for 10 nm process semiconductor and 10 G size large area process with high plasma density and VHF condition) funded by the Ministry of Knowledge Economy (MKE, Korea) and This research was supported by the MSIP (Ministry of Science, ICT and Future Planning), Korea, under the ITRC (Information Technology Research Center) support program (NIPA-2014-H0301-14-1007) supervised by the NIPA (National IT Industry Promotion Agency).

References and Notes

1. S. Y. Chou, P. R. Krauss, and P. J. Renstrom, *J. Vac. Sci. Technol. B* 101, 4129 (**1996**).
2. D.-Y. Khang, H. Kang, T.-I. Kim, and H. H. Lee, *Nano Lett.* 4, 633 (**2004**).
3. L. J. Heydermana, H. Schifta, C. Davida, J. Gobrechta, and T. Schweizerb, *Microelectronic Eng.* 54, 229 (**2000**).
4. M. Schvartzman and S. J. Wind, *Nanotechnology* 20, 145306 (**2009**).
5. Y. Kim, S. Kang, Y.-H. Ham, K.-H. Kwon, D. A. Shutov, H.-W. Lee, J. J. Lee, L.-M. Do, and K.-H. Back, *J. Vac. Sci. Technol. A* 30, 031601 (**2012**).
6. S. M. Rossnagel, J. J. Cuomo, and W. D. Westwood, Handbook of Plasma Processing Technology, Noyes Publications, New Jersey (**1990**).
7. J. R. Rooth, Industrial Plasma Engineering, IOP Publishing LTD, Philadelphia (**1995**).
8. S. Wolf and R. N. Tauber, Silicon Processing for the VLSI Era, Process Technology, Lattice Press, New York (**2000**), Vol. 1.
9. M. Ženkiewicz. *J. Achiev. Mater. Manuf. Eng.* 24, 137 (**2007**).
10. E. O. Johnson and L. Malter, *Phys. Rev.* 80, 58 (**1950**).
11. M. Sugavara, Plasma Etching: Fundamentals and Applications, Oxford University Press, New York (**1998**).
12. A. Efremov, N.-K. Min, B.-G. Choi, K.-H. Baek, and K.-H. Kwon, *J. Electrochem. Soc.* 155, D777 (**2008**).
13. A. Efremov, Y. Kim, H.-W. Lee, and K.-H. Kwon, *Plasma Chem. Plasma Proc.* 31, 259 (**2011**).
14. A. V. Vasenkov, X. Li, G. S. Oehrlein, and M. J. Kushner, *J. Vac. Sci. Technol. A* 22, 511 (**2004**).
15. S. Rauf and P. L. G. Ventzek, *J. Vac. Sci. Technol. A* 20, 14 (**2002**).
16. A. M. Efremov, D.-P. Kim, and C.-I. Kim, *Vacuum* 75, 133 (**2004**).

17. T. Kimura and M. Noto, *J. Appl. Phys.* 100, 063303 (**2006**).
18. T. Kimura and K. Ohe, *Plasma Sources Sci. Technol.* 8, 553 (**1999**).
19. D. Bose, S. Rauf, D. B. Hash, T. R. Govindan, and M. Meyyappan, *J. Vac. Sci. Technol. A* 22, 2290 (**2004**).
20. NIST Chemical Kinetics Database http://kinetics.nist.gov/kinetics/index.jsp.
21. M. A. Lieberman and A. J. Lichtenberg, Principles of Plasma Discharges and Materials Processing, John Wiley & Sons Inc., New York (**1994**).
22. T. Kimura and K. Hanaki, *Jpn. J. Appl. Phys.* 48, 096004 (**2009**).
23. W. W. Stoffels, E. Stoffels, and K. Tachibana, *J. Vac. Sci. Technol. A* 16, 87 (**1998**).
24. K. Miyata, M. Hori, and T. Goto, *Jpn. J. Appl. Phys.* 36, 5340 (**1997**).
25. C. Lee, D. B. Graves, and M. A. Lieberman, *Plasma Chem. Plasma Proc.* 16, 99 (**1996**).
26. A. M. Efremov, D. P. Kim, and C. I. Kim, *IEEE Transactions on Plasma Sci.* 32, 1344 (**2004**).
27. D. R. Lide, Handbook of Chemistry and Physics, CRC Press, New York (**1998–1999**).
28. X. Li, L. Ling, X. Hua, M. Fukasawa, G. S. Oehrlein, M. Barela, and H. M. Anderson, *J. Vac. Sci. Technol. A* 21, 284 (**2003**).
29. S. Kitova, M. Minchev, and G. Danev, *J. Optoel. Advanced Mater.* 7, 249 (**2005**).

Received: 8 December 2014. Accepted: 6 January 2015.